The Cryosphere Discuss., 6, 893–930, 2012
www.the-cryosphere-discuss.net/6/893/2012/
doi:10.5194/tcd-6-893-2012

The Cryosphere Discussions

Monte Carlo ice flow modeling projects a new stable configuration for Columbia Glacier, Alaska, by c. 2020

W. Colgan[1], W. T. Pfeffer[2], H. Rajaram[3], and W. Abdalati[1,4]

[1]Cooperative Institute for Research in Environmental Sciences, University of Colorado, Boulder, CO, 80309, USA
[2]Institute of Arctic and Alpine Research, University of Colorado, Boulder, CO, 80309, USA
[3]Department of Civil, Environmental, and Architectural Engineering, University of Colorado, Boulder, CO, 80309-0428, USA
[4]Headquarters, National Aeronautic and Space Administration, Washington, DC, 20546, USA

Received: 4 February 2012 – Accepted: 28 February 2012 – Published: 7 March 2012

Correspondence to: W. Colgan (william.colgan@colorado.edu)

Published by Copernicus Publications on behalf of the European Geosciences Union.

Abstract

Due to the abundance of observational datasets collected since the onset of its retreat (c. 1983), Columbia Glacier, Alaska, provides an exciting modeling target. We perform Monte Carlo simulations of the form and flow of Columbia Glacier, using a 1-D (depth-integrated) flowline model, over a wide range of parameter values and forcings. An ensemble filter is imposed following spin-up to ensure that only simulations which accurately reproduce observed pre-retreat glacier geometry are retained; all other simulations are discarded. The selected ensemble of simulations reasonably reproduces numerous highly transient post-retreat observed datasets with a minimum of parameterizations. The selected ensemble mean projection suggests that Columbia Glacier will achieve a new dynamic equilibrium (i.e. "stable") ice geometry c. 2020, by which time iceberg calving rate will have returned to approximately pre-retreat values. Comparison of the observed 1957 and 2007 glacier geometries with the projected 2100 glacier geometry suggests that, by 2007, Columbia Glacier had already discharged ~ 83 % of its total sea level rise contribution expected by 2100. This case study therefore highlights the difficulties associated with the future extrapolation of observed glacier mass loss rates that are dominated by iceberg calving.

1 Introduction

The observed rate of sea level rise over the 1993–2007 period was $3.3 \pm 0.4\,\mathrm{mm\,a^{-1}}$ (Cazenave and Llovel, 2010). The transfer of land-based ice into the ocean is now the leading cause of sea level rise (c.f. Bindoff et al., 2007), providing almost twice the contribution of the thermal expansion of sea water (~ 55 and 30 % of total sea level rise, respectively; Cazenave and Llovel, 2010). During the 1991–2002 period, small glaciers and ice caps (i.e. exclusive of the ice sheets) contributed $0.77 \pm 0.26\,\mathrm{mm\,a^{-1}}$ of sea level rise (Kaser et al., 2006). This is equivalent to ~ 25 % of the total sea level rise observed from all sources over the 1993–2007 period (Cazenave and Llovel,

TCD
6, 893–930, 2012

2010). While Patagonian glaciers currently have the most negative specific (i.e. per unit area) mass balance of glaciated regions exclusive of the ice sheets, Alaskan glaciers have the most negative total mass balance (Kaser et al., 2006). A comparison of digital elevation models suggests that Alaskan glaciers contributed $0.12 \pm 0.02\,\mathrm{mm\,a^{-1}}$ to sea level rise over the 1962–2006 period (Berthier et al., 2010). Laser altimetry observations indicate an Alaskan glacier sea level rise contribution of $0.27 \pm 0.10\,\mathrm{mm\,a^{-1}}$ between 1992 and 2002 (Arendt et al., 2002). This latter contribution rate, however, is considered an overestimate, due to the extrapolation of glacier centerline altimetry data to less dynamically active ice-covered areas (Berthier et al., 2010). The Alaskan glacier contribution to sea level rise has also been examined in several gravimetry studies. Chen et al. (2006) suggested a contribution of $0.28 \pm 0.06\,\mathrm{mm\,a^{-1}}$ over the 2002–2005 period (converted from $101 \pm 22\,\mathrm{km^3\,a^{-1}}$). Luthcke et al. (2008) subsequently suggested a contribution of $0.23 \pm 0.01\,\mathrm{mm\,a^{-1}}$ over the 2003–2007 period. Most recently, Jacobs et al. (2012) have suggested a contribution of $0.13 \pm 0.02\,\mathrm{mm\,a^{-1}}$ over the 2003–2010 period (converted from $47 \pm 7\,\mathrm{Gt\,a^{-1}}$). Together, these observations suggest that the Alaskan contribution is equivalent to ∼ 35 % of the total small glacier and ice cap contribution to sea level rise over 1993–2005 period (Kaser et al., 2006), and ∼ 8 % of the total observed sea level rise over the 1993–2007 period (Cazenave and Llovel, 2010).

Of all Alaskan Glaciers, Columbia Glacier is presently the single largest contributor to sea level rise (Arendt et al., 2002; Berthier et al., 2010). Over the 1995–2001 period, Columbia Glacier contributed $\sim 7.1\,\mathrm{km^3\,a^{-1}}$ of water to sea level rise, equivalent to ∼ 0.6 % of total observed sea level rise over the 2003–2007 period (Arendt et al., 2002; Cazenave and Llovel, 2010). Prior to the c. 1983 onset of its rapid and ongoing retreat, Columbia Glacier had an area of $\sim 1070\,\mathrm{km^2}$ and a length of ∼ 66 km (Meier et al., 1985; Krimmel, 2001). The pre-retreat terminus position, first documented in 1794, is believed to have been stable since the 15th century (Rasmussen et al., 2011). Since 1983, Columbia Glacier has retreated ∼ 18 km and lost $\sim 100\,\mathrm{km^2}$ of ice covered area from its terminus (Fig. 1). This rapid retreat has been well-documented,

TCD
6, 893–930, 2012

which makes Columbia Glacier an exciting modeling target. Observational datasets suitable for model validation include: (i) the pre-retreat ice surface elevation profile (Meier et al., 1985), (ii) the pre-retreat ice surface velocity profile (Meier et al., 1985), (iii) the contemporary surface mass balance profile and equilibrium line altitude (Mayo, 1984; Rasmussen et al., 2011), (iv) a time-series of terminus position (Krimmel, 2001), (v) a time-series of iceberg calving rate (Krimmel, 2001; Rasmussen et al., 2011), and (vi) a time-series of surface ice velocity at $\zeta = 50$ km (where ζ is the curvilinear coordinate system describing downstream distance on Columbia Glacier's main flowline; Fig. 1; Krimmel, 2001).

We examine the past and future behavior of Columbia Glacier using a 1-D (depth-integrated) flowline model that incorporates longitudinal coupling stresses and uses statistical parameterizations for two important, but poorly understood, processes: basal sliding and iceberg calving. In Monte Carlo fashion we execute the model a large number of times, over a wide parameter space, to identify the cumulative uncertainty associated with both parameter and forcing uncertainties, and to provide robust ensemble mean histories and projections of variables of interest. We use an ensemble filtering technique to eliminate unrealistic simulations, whereby specific simulations are discarded if they do not: (i) satisfactorily reproduce observations of ice thickness (a state variable) at the conclusion of a transient spin-up, or (ii) initiate retreat within 100 yr of the onset of a transient forcing. Similar Monte Carlo selection approaches have been used extensively in the context of oceanic (e.g., Van Leeuwen and Evensen, 1996) and atmospheric (e.g., Anderson and Anderson, 1999) modeling. In glaciology, Monte Carlo simulations have been used to explore uncertainty in surface mass balance parameters (Machguth et al., 2008; Gardner et al., 2011). We find that the aforementioned diverse observational datasets are reasonably well reproduced by the selected ensemble of simulations. When projected into the future, the selected ensemble mean simulation indicates that Columbia Glacier will achieve a new dynamic equilibrium geometry (i.e. "stable" position), and hence no longer significantly contribute to sea level rise, by c. 2020. Thus, this case study suggests that caution must be exercised in the

TCD
6, 893–930, 2012

future extrapolation of contemporary mass loss rates that are dominated by iceberg calving rate (a transient variable).

2 Methods

2.1 Ice flow model

We apply a previously published (Colgan et al., 2012) depth-integrated (1-D) flowline model with a higher order approximation for longitudinal coupling stresses to the main centerline of Columbia Glacier. The model domain of the center flowline of Columbia Glacier extends from the main flow divide at ~2750 m elevation at km 0 (61.369° N and 147.153° W) down to sea level at km 70 (60.974° N and 147.093° W; Fig. 1). The model solves for the transient rate of change in ice thickness ($\partial H/\partial t$) according to mass conservation:

$$\frac{\partial H}{\partial t} = b - \frac{1}{w}\frac{\partial Q}{\partial x} \tag{1}$$

where b is annual surface mass balance, w is the glacier width and $\partial Q/\partial x$ is the along-flowline divergence of ice discharge. Following Marshall et al. (2005), depth-integrated ice discharge (Q) is taken as:

$$Q = F w \left(u_b H + \frac{2A}{(n+2)} \left(\rho g \left| \frac{\partial z_s}{\partial x} \right| \right)^{(n-1)} \tau H^{(n+1)} \right) \tag{2}$$

where F is a spatially variable dimensionless shape factor, u_b is the basal sliding velocity, A is the flow law parameter (we assume that Columbia Glacier is at the pressure-melting-point throughout and take A as 1.4×10^{-16} Pa^{-3} a^{-1}; O'Neel et al., 2005), n is the flow law exponent (taken as 3), ρ is the density of ice (taken as 900 kg m^{-3}), g is gravitational acceleration (taken as 9.81 m s^{-2}), $\partial z_s/\partial x$ is the ice surface slope between adjacent nodes and τ is total driving stress (the sum of both gravitational

TCD
6, 893–930, 2012

and longitudinal coupling stresses). In an approximation of the momentum balance, depth-averaged longitudinal coupling stress ($\overline{\tau}'_{xx}$) is included as a perturbation to the gravitational driving stress (Van der Veen, 1987; Marshall et al., 2005):

$$\tau = -\rho g H \frac{\partial z_s}{\partial x} + 2\frac{\partial}{\partial x}\left(H\overline{\tau}'_{xx}\right) \tag{3}$$

Depth-averaged longitudinal coupling stress is calculated following the approach outlined by Van der Veen (1987). This formulation derives longitudinal coupling stress by solving a cubic equation describing equilibrium forces independently at each node, based on ice geometry and prescribed basal sliding velocity:

$$0 = \overline{\tau}'^{\,3}_{xx}\left\{2\frac{\partial z_s}{\partial x}\left(\frac{\partial H}{\partial x} - \frac{\partial z_s}{\partial x}\right) + H\frac{\partial^2 z_s}{\partial x^2} - \frac{1}{2}\right\} + \overline{\tau}'^{\,2}_{xx}\left\{\tau\left(\frac{2}{3}\frac{\partial H}{\partial x} - \frac{3}{2}\frac{\partial z_s}{\partial x}\right)\right\} + \ldots \tag{4}$$

$$\overline{\tau}'_{xx}\left\{\tau^2\left(3\frac{\partial z_s}{\partial x}\frac{\partial H}{\partial x} + \frac{3}{2}H\frac{\partial^2 z_s}{\partial x^2} - 2\left(\frac{\partial z_s}{\partial x}\right)^2 - \frac{1}{6}\right)\right\} + \tau^3\left(\frac{2}{5}\frac{\partial H}{\partial x} - \frac{1}{4}\frac{\partial z_s}{\partial x}\right) + \frac{1}{2A}\frac{\partial u_b}{\partial x}$$

The spatially variable shape factor (F) is prescribed as a function of glacier width following Paterson (1994, p. 269). We interpolate glacier width (w; Eqs. 1 and 2) from the distance measured between lateral shear margins along the main flowline of Columbia Glacier in the 1 : 100 000 Plate 5 map of Meier et al. (1985; Fig. 2). Making the now common assumption that the contribution of internal deformation to surface ice velocity is negligible in the ablation zone of Columbia Glacier (i.e. downstream of km ~ 40; Kamb et al., 1994; Pfeffer, 2007) allows us to implement a statistical parameterization of basal sliding velocity. This empirical, and hence site specific, parameterization is predicated on the observation that ice surface velocity profiles observed over the 1981 to 2001 period (Pfeffer, 2007) can be approximated with a simple exponential curve of the form:

$$u_b = k e^{(x/\alpha)} \tag{5}$$

TCD
6, 893–930, 2012

where k is a dimensional coefficient of $1\,\mathrm{m\,a^{-1}}$, x is the distance downstream from km 0 and α is a scaling length (Fig. 3). This basal sliding prescription is not a sliding rule, whereby basal sliding velocity is parameterized to vary with glacier geometry or hydrology, but rather a curve fit of observed sliding velocity as a function of flowline distance (x); similar to a curve fit of surface ablation as a function of elevation (z; Eq. 6). Observations indicate that α ranged between ~ 8.9 km in 1981 and ~ 5.8 km in 2001 (i.e. depending on terminus position). We prescribe α as a function of terminus position (x_{term}), which allows α to decrease as the terminus retreats upstream. We assume that α reaches a minimum of 5.25 km when the terminus reaches km 50, the approximate upstream limit of the bedrock over-deepening of the main flowline of Columbia Glacier (McNabb et al., 2012). In each Monte Carlo simulation we randomly perturb α by a value uniformly distributed between −0.25 and +0.25 km. As α resides in an exponent, this parameter range yields a wide variety of basal sliding profiles for a given terminus position. For example, perturbing the 1992 velocity profile approximation by $\alpha = 6.8 \pm 0.25$ km results in an ensemble velocity range of $\sim \pm 1.0\,\mathrm{km\,a^{-1}}$ at km 55, and $\sim \pm 2.5\,\mathrm{km\,a^{-1}}$ at km 60 (Fig. 3).

Similar to Nick et al. (2007), we parameterize annual surface mass balance (b) as a linear function of ice surface elevation (z_{s}) according to:

$$b = \begin{cases} \gamma(z_{\mathrm{s}} - z_{\mathrm{ela}}) & \text{if } b < b_{\mathrm{max}} \\ b_{\mathrm{max}} & \text{if } b \geq b_{\mathrm{max}} \end{cases} \quad (6)$$

where γ is the observed annual surface mass balance gradient ($\Delta b / \Delta z_{\mathrm{s}}$; taken as $0.0085\,\mathrm{a^{-1}}$; Rasmussen et al., 2011), z_{ela} is the equilibrium line altitude, and b_{max} is the maximum surface mass balance (i.e. accumulation or snowfall) rate. Randomly prescribing z_{ela} from a uniform distribution between 850 and 1050 m and b_{max} from a uniform distribution between 4.5 and $6.0\,\mathrm{m\,a^{-1}}$ yields a range of surface mass balance profiles that agree well with observations (Mayo, 1984; Rasmussen et al., 2011; Fig. 4). During spin-up, z_{ela} is prescribed as 200 m lower than the contemporary range (i.e. from a uniform distribution between 650 and 850 m) to simulate the cooler climate

TCD
6, 893–930, 2012

with which pre-retreat Columbia Glacier was most likely in equilibrium (Nick et al., 2007).

2.2 Climatic variability and forcing

In order to simulate natural climatic variability, we introduce a stochastic element by allowing equilibrium line altitude to randomly vary each decade (i.e. $z_{ela} \pm \delta z_{ela}$). The magnitude of the decadal perturbation (δz_{ela}) is randomly selected from a distribution derived from reanalysis data (Compo et al., 2011). We assume that annual z_{ela} variability ($\Delta z_{ela}/\Delta t$) may be approximated by dividing annual air temperature variability ($\Delta T/\Delta t$) by local environmental lapse rate ($\Delta T/\Delta z$) at equilibrium line altitude:

$$\frac{\Delta z_{ela}}{\Delta t} = \left(\frac{\Delta T}{\Delta t}\right)\left(\frac{\Delta T}{\Delta z}\right)^{-1} \quad (7)$$

This assumes that equilibrium line altitude is correlated with a given isotherm during the melt season (Andrews and Miller, 1972). In order to determine appropriate values of $\Delta T/\Delta t$ and $\Delta T/\Delta z$, we extract 137-yr time-series of 900 and 950 mb melt season (1 April to 30 September) air temperature at Columbia Glacier from 20th Century Reanalysis V2 Data (Compo et al., 2011; Fig. 5). The 900 mb pressure level corresponds to ~ 990 m elevation, the approximate equilibrium line altitude of Columbia Glacier over the 137-yr period. Reanalysis data suggests that during the 1871 to 2008 period, the mean local environmental lapse rate ($\Delta T/\Delta z$) was 6.7 K km^{-1}, and the annual variability in 900 mb air temperature ($\Delta T/\Delta t$) exhibited an approximately normal distribution centered on 0 K a^{-1} (Fig. 5 inset). Dividing this annual $\Delta T/\Delta t$ distribution by the mean local environmental lapse rate yields a distribution of annual z_{ela} variability ($\Delta z_{ela}/\Delta t$; Eq. 7). We convert this annual $\Delta z_{ela}/\Delta t$ distribution into a decadal $\Delta z_{ela}/\Delta t$ distribution by applying a 10-yr running mean to 10 000 yr of synthetic z_{ela} variability generated using the annual $\Delta z_{ela}/\Delta t$ distribution (Fig. 6). This synthetic data suggests that decadal z_{ela} perturbations (δz_{ela}) can be described by a normal distribution with a mean of 0 m and a standard deviation of 30 m.

TCD
6, 893–930, 2012

During transient spin-up, equilibrium line altitude is perturbed each decade around a fixed mean z_{ela}. During the subsequent transient forcing period, however, the mean z_{ela} is also forced upwards based on the long-term air temperature trend ($\Delta T/\Delta t$). The long-term trend in $\Delta T/\Delta t$ is taken as the linear trend in the 900 mb air temperature over the 1871 to 2008 period (Compo et al., 2011). In each Monte Carlo simulation, long-term $\Delta T/\Delta t$ is randomly prescribed from a uniform distribution between 0.0057 and 0.0262 K a^{-1}. This range corresponds to the minimum and maximum trends (i.e. trend ± standard slope error) in air temperature over the 1871 to 2008 period (dashed lines Fig. 5). Dividing this rate of air temperature increase ($\Delta T/\Delta t$) by local environmental lapse rate ($\Delta T/\Delta z$) yields the rate of z_{ela} increase ($\Delta z_{ela}/\Delta t$) imposed during the transient forcing period (Eq. 7). This future climate forcing conservatively assumes no acceleration in the contemporary rate of increase in air temperature.

2.3 Model implementation and boundary conditions

The flowline model we apply to the main centerline of Columbia Glacier is depth-integrated (i.e. 1-D; Colgan et al., 2012). The differential equations describing transient ice thickness ($\partial H/\partial t$) were discretized in space using first-order finite volume methods ($\Delta x = 250$ m). The semi-discrete set of ordinary differential equations was then solved using "ode15s", the stiff differential equation solver in MATLAB R2008b with a time-step (Δt) of 1 yr. The model was optimized to run on 8 parallel processors using the parallel computing toolbox in MATLAB R2008b. The mean processor time per Monte Carlo simulation was ~58 s (Fig. 7). This allowed the 5000 simulations to be completed in ~10 wall-clock hours using a 750 W Dell PowerEdge 2950 server with eight 2.83 GHz processors and a total of 32 GB of RAM.

The model ice geometry is initialized with observed pre-retreat ice surface elevation (Meier et al., 1985) and inferred bedrock elevation (McNabb et al., 2012). The basal (bottom) boundary condition is a prescribed basal sliding velocity (Eq. 5), while the surface (top) boundary condition is a prescribed surface mass balance (Eq. 6). The upstream (left) boundary condition is a second-type (prescribed flux) Neumann boundary

TCD
6, 893–930, 2012

condition to simulate an ice flow divide (i.e. $Q = 0$ at $x = 0$ km). The downstream (right) boundary condition at the glacier terminus is a first-type (prescribed head) Dirichlet boundary condition, as the ice discharge at the terminal node (Q_{term}) is not known. This empirical, and hence site-specific, downstream boundary condition is based on the observation that mean terminus ice cliff height over the 1981 to 2001 period was 80 m (Pfeffer, 2007). Thus, at the conclusion of a time step, terminus position is explicitly updated as the node downstream of which ice surface elevation is < 80 m; all ice downstream of this node is prescribed to calve. While this calving parameterization honors the observed terminus ice cliff height of Columbia Glacier, we acknowledge that it is not physically based (c.f. calving rate as a function of longitudinal strain-rate; Nick et al., 2010). We note that an overarching goal of the Monte Carlo ensemble filter approach is to explore the response of a diverse population of Columbia Glaciers to a range of transient forcings, rather than to replicate or isolate an individual process. Thus, similar to the basal sliding and surface mass balance parameterizations we prescribe, a site-specific empirical calving parameterization facilitates our exploration of stable and unstable states of Columbia Glacier.

Total iceberg calving rate (D) is taken as the sum of both transient ice discharge through the terminal node (Q_{term}) and the prescribed change in terminus position due to imposed iceberg calving:

$$D = Q_{\text{term}} + \frac{\Delta x}{\Delta t} \sum (H_i w_i \mathcal{H}(x_i - x_{80})) \tag{8}$$

where subscript i denotes node index, and is a dimensionless Heaviside function of the form:

$$\mathcal{H}(x_i - x_{80}) = \begin{Bmatrix} 1 & \text{for} & x_i \geq x_{80} \\ 0 & \text{for} & x_i < x_{80} \end{Bmatrix} \tag{9}$$

where x_{80} is the location where $z_s = 80$ m.

While the inclusion of a dimensionless shape factor (F) implicitly accounts for divergence and convergence stemming from changes in flowband width, it does not

TCD
6, 893–930, 2012

account for the influence of tributaries. The main flowline of Columbia Glacier receives discharge from three major tributaries: "west" at km ~ 51, "east" at km ~ 38 and "main-west" at km ~ 29 (Fig. 1). We account for tributary effects by increasing ice inflow at the junction of each tributary by an amount proportional to the main flowline ice discharge. This additional ice inflow is smoothly distributed over several adjacent nodes using a Gaussian curve (1 km standard deviation). We increase ice inflow by temporally invariant tunable factors of 80, 25 and 40 % at km 29, 38 and 51, respectively. While these factors are imposed at tributary junctions, they represent the additional ice inflow not only from the tributary, but also the numerous smaller glaciers and cirque basins between tributaries. For example, a comparison of the main and main-west pre-retreat centerline velocities (600 and 300 m a^{-1}, respectively; Meier et al., 1985) suggests main-west likely contributed an additional 50 % ice inflow to the main flowline at km 29. There are, however, ~ 6 smaller glaciers/cirque basins between km 0 and 29, which we estimate to contribute the remaining 30 % additional ice discharge at km 29.

2.4 Monte Carlo ensemble filtering

We executed a large number of model simulations (5000) in order to provide a robust ensemble mean projection of specific variables of interest, and also assess the cumulative effect of both parameter and forcing uncertainties. We randomly varied three key model parameters over a wide parameter space, two of which influence surface mass balance (b_{max} and z_{ela}), and one which influences ice flow (scaling length in the basal sliding parameterization: α). We also randomly varied the main forcing parameter, rate of increase in 900 mb air temperature ($\Delta T/\Delta t$). Each simulation begins with a 500-yr fully transient spin-up. At the conclusion of this 500-yr spin-up, the first ensemble selection filter was imposed: only simulations that reproduced observed pre-retreat (i) mean ice surface elevation between km 40 and 60 to within ±100 m (Meier et al., 1985) and (ii) terminus position (x_{term}) to within ±2.5 km (Meier et al., 1985) were selected to carry forward into a 250-yr transient forcing period. Simulations that did not satisfactorily reproduce features (i) and (ii) were discarded. The wide parameter space of the selected

TCD
6, 893–930, 2012

ensemble of simulations produced a population of modeled Columbia Glaciers of varying "sensitivities" (where "sensitivity" is broadly defined as mean ice reservoir overturn time in the spirit of Johannesson et al., 1989). Relatively high basal sliding and surface accumulation simulations yielded glaciers with lower mean ice reservoir overturn time than relatively low basal sliding and surface accumulation simulations (i.e. both types of simulations produced acceptable pre-retreat geometries but with different sensitivities). During the subsequent 250-yr transient forcing period, this selected population of glaciers was forced by a wide range of rates of increase in equilibrium line altitude. A second ensemble selection filter was imposed to discard simulations in which retreat did not initiate within 100 yr of forcing onset. As retreat initiated at different times between simulations, the floating model time of the twice selected simulations (i.e. those which accurately reproduced pre-retreat glacier geometry and initiated retreat within 100 yr of forcing onset), was transposed to real time by a least-squares fit between modelled and observed terminus position histories. Subjecting the selected population of glaciers, with varying climatic sensitivities, to a wide range of climatic forcings produced a robust ensemble mean history (and projection) for a number of observable variables including: equilibrium line altitude, terminus position, velocity at km 50 and iceberg calving rate. The spread across the selected ensemble provides a robust measure of the cumulative uncertainty resulting from both parameter and forcing uncertainties.

3 Results

Of the 5000 Monte Carlo simulations initialized, 1882 (~ 38 %) were selected at the end of transient spin-up, based on the accurate reproduction of pre-retreat ice geometry, to carry forward into the 250-yr transient forcing period. The 3118 simulations (~ 62 %) that failed to reproduce observed pre-retreat ice geometry at the end of spin-up were discarded (i.e. not included in the transient forcing ensemble). Of the 1882 selected simulations, 175 were discarded by the second selection filter (~ 9 %), as they did

TCD
6, 893–930, 2012

not exhibit a retreat within 100 yr of the onset of forcing. Thus, only 1707 simulations (∼35 % of the original 5000) passed both ensemble selection filters. An inherent trade-off exists between the number of simulations selected and the size of the parameter space; a larger parameter space decreases the probability that a given simulation will achieve selection criteria but increases the robustness of the ensemble mean. The selected simulations contain the full range of initial equilibrium line altitude values (650 to 850 m) and maximum surface mass balance values (4.5 to 6.0 m a^{-1}) over a wide range of basal sliding velocities (Fig. 8). The population of selected simulations appears to exhibit a preference for high sensitivity simulations (i.e. relatively high maximum surface mass balance (or accumulation) and basal sliding values and relatively low equilibrium line altitude) in comparison to low sensitivity simulations (i.e. relatively low maximum surface mass balance (or accumulation) and basal sliding values and high equilibrium line altitude).

Both the ice surface elevation and velocity profiles of the selected simulations at the conclusion of transient spin-up (taken to be representative of the pre-retreat profiles) compare well with 1977/78 observed ice surface elevation and velocity profiles interpolated at every second kilometer along the main flowline of Columbia Glacier (Meier et al., 1985; Fig. 9). While the ensemble mean modeled velocity profile generally captures the shape of the observed velocity profile, some discrepancies exist. Firstly, the modeled profile fails to capture the localized velocity influence of an icefall at km ∼ 23. The failure of the model to adequately represent the complex physics at an icefall, where significant crevassing occurs, likely stems from the momentum balance approximation employed: the assumption of continuum mechanics is not valid where ice becomes discontinuous. Secondly, the modeled profile underestimates surface ice velocity in the vicinity of km 35. This is likely due to an underestimation of local convergence. This suggests that the measured distance between lateral shear zones may not be a good proxy for glacier channel width in the vicinity of km 35. Finally, the modeled ice velocity at km 66 (the terminus) fails to achieve the velocity assessed by Meier et al. (1985). As the 1977/78 velocity observations downstream of km ∼ 62 are not in situ,

TCD
6, 893–930, 2012

but rather extrapolated from upstream photogrammetric values (Meier et al., 1985), we regard this slight mismatch as reasonable.

In addition to achieving very good agreement with observed pre-retreat ice surface elevation and velocity profiles, the modeled ensemble mean time-series of equilibrium line altitude, terminus position, ice velocity at km 50 and calving rate also agree well with observed records (Mayo, 1984; Krimmel, 2001; Rasmussen et al., 2011; Fig. 11). The combination of (i) a 200 m depression of equilibrium line altitude to simulate "cooler" climate during spin-up, and (ii) an air temperature forcing of between 0.0057 and 0.0262 $K\,a^{-1}$ (combined with a mean local environmental lapse rate of 6.7 $K\,km^{-1}$), produces an ensemble mean equilibrium line altitude that agrees very well with observed contemporary equilibrium line altitude. If climate forcing persists at its current rate, the equilibrium line altitude at Columbia Glacier will be ~ 1200 m by the year 2100.

The ensemble mean suggests that Columbia Glacier will achieve a new stable terminus position at km ~ 42 (near the grounding line) by c. 2020, and maintain this terminus position until at least 2100 (Fig. 11). The modeled time-series of transient terminus position may suggest a slightly faster retreat than observed. We regard any discrepancy in retreat rate as within uncertainty across the ensemble (i.e. observations lie within the envelope of Monte Carlo simulations), and discuss possible causes and interpretations of a slight mismatch in Sect. 4. Differences between the 1977/78 and 2100 ice surface elevation and velocity profiles are generally restricted to the region downstream of the km 23 icefall (c.f. Figs. 9b,d and 10). The absence of significant changes to ice geometry and velocity upstream of the km 23 icefall over the remainder of the century is noteworthy.

The ensemble mean time-series of surface ice velocity at km 50 generally reproduces the broad features (i.e. the sign and magnitude) of the observed local velocity record at km 50 (Krimmel, 2001; Fig. 11). The ensemble of simulations indicate that the surface ice velocity at km 50 increases by a factor of between 2.5 and 5.0, relative to pre-retreat (i.e. 1977/78) velocities, between the onset of retreat and the time when the

TCD
6, 893–930, 2012

terminus retreats upstream of km 50. The finer features of the km 50 velocity record, however, such as the precise timing of acceleration and temporal velocity inflections, are not well reproduced. Given that surface ice velocity essentially reflects basal sliding velocity in the ablation zone of Columbia Glacier (Kamb et al., 1994; Pfeffer, 2007), and the rather simple basal sliding parameterization employed in this study (Eq. 5), the agreement between observed and modeled ice velocity at km 50 is reasonable.

The ensemble mean iceberg calving rate time-series suggests that iceberg calving will "turn off" (i.e. return to dynamic equilibrium values) c. 2020, when a new stable terminus position is achieved, just as quickly as iceberg calving "turned on" at the initiation of retreat c. 1983 (Fig. 11). Thus, the total response time (i.e. period of highly transient behavior) of Columbia Glacier to the retreat initiated by contemporary climate forcing is expected to be ~ 40 yr. There is very good agreement between ensemble mean modeled and observed iceberg calving rate until c. 1995. After c. 1995, modeled calving rate remains generally constant at $\sim 63\,\%$ of the observed value (Rasmussen et al., 2011), until c. 2005, when it begins a rapid decrease to pre-retreat rates. There are several factors potentially contributing to this discrepancy. Firstly, the relative decrease in modeled iceberg calving rate coincides with the c. 2001 minima in both terminal flowline width (w) and shape factor (F; Fig. 12). Any potential error in F and w is multiplied (i.e. compounded) when calculating the iceberg calving rate (Eqs. 2 and 8). Thus, we interpret the discrepancy as suggesting that the prescribed flowline width (and hence shape factor) does not sufficiently represent the complexities of ice flow in the km 50 to 60 portion of the flowline. The difficulties associated with modeling ice flow through the Kadin-Great Nunatak (K-GN) constriction at km ~ 53 (Fig. 1) are further discussion in Sect. 4.

Secondly, in addition to being subject to uncertainties in w and F, the calving term also incorporates two statistical parameterizations (basal sliding velocity and terminus change due to iceberg calving), and compounds the uncertainty in both parameterizations. While these statistical parameterizations achieve satisfactory first-order agreement with ice geometry and velocity observations, they are undeniably less robust than

TCD
6, 893–930, 2012

first-principles physically-based parameterizations. For example, recent digital photographic analysis (E. Welty, personal communication) suggests an ice cliff height of closer to ∼100 m when the terminus was in the K-GN gap. Matching the observed surface velocity profile with a parameterized 80 m ice cliff height can therefore be expected to result in an proportional underestimation of calving flux (i.e. 8/10 of actual calving flux). Finally, part of the discrepancy between modeled and observed calving rate is due to the fact that the observed rate pertains to the entire Columbia Glacier complex (i.e. both the west and main branches), while the modeled calving rate only applies to the main branch once the terminus retreats upstream of the km 51 confluence. This distinction, however, should only result in discrepancy after c. 2005 (when the terminus position retreats upstream of km 51).

4 Discussion

4.1 Model limitations

While six diverse observed datasets ((i) pre-retreat ice surface elevation profile, (ii) pre-retreat ice surface velocity profile, (iii) contemporary surface mass balance profile and equilibrium line altitude, (iv) time-series of terminus position, (v) time-series of iceberg calving rate and (vi) time-series of surface ice velocity at km 50 following the onset of retreat) are reasonably well reproduced by the model, the 1-D flowline model suffers from inherent limitations in the treatment of: (i) lateral effects (i.e. convergence/divergence due to complex bed topography/tributaries) and (ii) ice density. Complex lateral effects stemming from bed topography are a significant issue in the vicinity of the K-GN bedrock constriction at km 53. The observed record of terminus position indicates that the retreat of Columbia Glacier slowed down for ∼5 yr at the K-GN bedrock constriction (Fig. 1). The modeled terminus retreat, however, does not exhibit this temporary slowdown, and continues at a relatively constant rate through the constriction (Fig. 11). The lateral effects stemming from bedrock topography at the

TCD
6, 893–930, 2012

constriction are complicated by the lateral effects stemming from the confluence of the west tributary at the same approximate location (km 50 to 53).

The K-GN bedrock constriction is represented in the model by a minimum glacier width of 3 km prescribed at km 53, based on the distance between lateral shear margins in the 1977/78 ice surface velocity map (Meier et al., 1985; Fig. 2). More recent (2010) Landsat imagery reveals that the bedrock channel width at sea level is closer to 2 km (Fig. 1). Thus, the effective glacier width has experienced a significant decrease (by $\sim 33\,\%$) in the vicinity of the K-GN gap since the onset of the retreat. Changes in glacier width over the retreat period are not as pronounced elsewhere along the flowline. While employing a transient shape factor that is dependent on ice thickness (i.e. $F(w(H(t)))$ rather than $F(w)$) may offer some potential to refine the treatment of a bedrock constriction in a flowline model, it would not improve the treatment of tributary convergence. A 2-D (plan view) model offers a better potential to improve the treatment of the bedrock constriction than further parameterization of a 1-D (flowline) model. Generally, however, even with 1-D limitations of lateral effects, the ice geometry and timing of retreat is reasonably well reproduced as the glacier retreats through the bedrock constriction.

Similar to previous Columbia Glacier modeling investigations (O'Neel et al., 2005; Nick et al., 2007) we assume that ice density is constant in space and time (taken as $900\,\mathrm{kg\,m^{-3}}$). At Columbia Glacier, however, observations suggest that heavy crevassing can result in extremely low bulk ice densities in the ablation zone (e.g. $< 700\,\mathrm{kg\,m^{-3}}$ in the top 85 m of ice at km 63.7; Meier et al., 1994). Furthermore, these observations, as well as anecdotal evidence, suggest that the ablation zone of Columbia Glacier has become progressively more crevassed since the retreat begin c. 1983 (Meier et al., 1994). Continuity calculations suggest that ice density decreases by $\sim 20\,\%$ as ice flows downstream from the bedrock constriction at km 53 to the glacier terminus, achieving depth-averaged bulk ice densities as low as $750\,\mathrm{kg\,m^{-3}}$ (Venteris, 1997). Thus, in reality, ice density at Columbia Glacier is neither constant in time nor space. This has important consequences for an ice flow model of the type used in this,

TCD
6, 893–930, 2012

and many other, studies (i.e. a model predicated on continuum mechanics and mass conversation with invariant density). For example, an increase in bulk ice density over time would result in an increase in ice volume over time, which would decrease the apparent modeled rate of terminus retreat (i.e. the upstream migration of the terminus due to calving would be offset by the volumetric expansion of remaining ice). Spatially and temporally transient ice density, however, is not even incorporated in the most sophisticated ice flow models, including Elmer (Gagliardini and Zwinger, 2008), Community Ice Sheet Model (CISM; Lipscomb et al., 2009) and Parallel Ice Sheet Model (PISM; Winkelmann et al., 2011).

4.2 Projecting sea level rise

Forecasting the cryospheric contribution to sea level rise over the next century is a task of paramount importance for the glaciology community. At present, physically-based projections of the small glacier and ice cap contribution to global sea level rise have been restricted to the surface mass balance component (Raper and Braithwaite, 2006; Radić and Hock, 2011), ignoring the potential contribution due to ice dynamics (primarily due to the computational expense associated with solving the transient equations for ice flow for a large population of glaciers). Statistically-based projections of total mass balance have been applied to both ice sheets (e.g., Velicogna, 2009; Rignot et al., 2011) and small glaciers and ice caps (e.g., Meier et al., 2007). These projections extrapolate future sea level rise contributions from trends contained in the observed record. Our present study of Columbia Glacier serves as a reminder that caution should be exercised when performing such statistical projections (e.g., Price et al., 2011). While the absolute magnitude of our modeled iceberg calving rate does not agree precisely with observations after c. 1995, the good agreement between observed and modeled ice geometry and velocity lends high confidence to the general timing and shape of iceberg calving rate projection. Thus, it is very likely that the iceberg calving rate of Columbia Glacier will indeed "turn off" (i.e. return to a stable dynamic equilibrium value) by c. 2020 just as quickly as it "turned on" c. 1983 (Fig. 11).

TCD
6, 893–930, 2012

This exemplifies how a statistical extrapolation of pre-2000 trends into the post-2000 period could lead to erroneous projections. As iceberg calving rate is not a "state" variable (i.e. a variable capable of predicting the future behavior of a system), extrapolating past mass loss rates that are primarily based on iceberg calving is not robust, as rapid changes in ice dynamics can result in decade-scale transitions between stable and unstable states.

We estimate the remaining response of Columbia Glacier to the rapid retreat initiated c. 1983 by comparing the total sea level rise contributions of the model domain in the 2007–2100 and 1957–2100 periods (Fig. 10). We can calculate the total anticipated sea level rise contribution from the model domain (i.e. the main flowline of Columbia Glacier) between 2007 and 2100 by quantifying the difference in ice volume (δV) between the observed 2007 ice thickness (H_{2007}; McNabb et al., 2012) and the ensemble mean modeled 2100 ice thickness (H_{2100}), according to:

$$\delta V = \int w(x)(H_{2100}(x) - H_{2007}(x)) \cdot dx \tag{10}$$

This formulation projects a total sea level rise contribution of 15.1 km^3 from the main flowline model domain over the 2007 to 2100 period. This estimate excludes all ice covered areas outside the main flowline model domain (i.e. adjacent small glaciers, cirques and tributaries). An analogous calculation with the 1957 ice thickness (McNabb et al., 2012) indicates a total comparable sea level rise contribution of 88.7 km^3 over the 1957 to 2100 period. Differencing these values suggests that, by 2007, Columbia Glacier had already discharged ~ 83 % of the total sea level rise contribution anticipated by 2100 (i.e. 73.6 of 88.7 km^3; Fig. 10). As the pseudo area of the 1-D flowline model (i.e. $\int w(x) \cdot dx$) is only a fraction of the total ice-covered area of the Columbia Glacier complex (~ 260 of ~ 910 km^2; McNabb et al., 2012), these numbers are gross underestimates of the absolute values of the sea level contribution of the entire ice complex (which was 160 km^3 over the 1957–2007 period; McNabb et al., 2012). They do, however, illustrate that the majority of the response of Columbia Glacier to the

TCD
6, 893–930, 2012

terminus perturbation initiated c. 1983 has probably been completed. While this exercise is similar to the concept of "committed sea level rise" (Price et al., 2011), it differs slightly by maintaining a climate forcing throughout the entire transient simulation.

This study demonstrates that Columbia Glacier has a multi-decadal response time (i.e. ∼40 yr), which is likely a function of the length of the marine-grounded reach as well as total basin size, and is expected to achieve a new dynamic equilibrium well in advance of 2100 (i.e. c. 2020). If these characteristics are representative of other Alaskan tidewater glaciers, a computationally efficient means of projecting the Alaskan tidewater glacier sea level rise contribution by 2100 may be achieved by calculating glacier volumes in steady-state with year 2100 climate (e.g. "post-collapse equilibrium profiles" of Bamber et al., 2009). Making the assumption that tidewater glaciers will be in steady-state with the 2100 climate reduces the tremendous computational expenditure of numerically solving the transient equations governing ice flow through spin-up and forcing, to a single (i.e. instantaneous) solution of the continuity equation. This assumption would be valid when the response time is a fraction of the projection period of interest (i.e. the response can be assumed to be complete at a given time in the future). The response time of land-terminating glaciers is recognized to be proportional to ice volume, and has been approximated as the mean ice thickness of a glacier divided by the mean absolute ablation rate below the equilibrium line (Johannessson et al., 1989). A similar first-order approximation of response time has not been proposed for tidewater glaciers. Thus, employing a steady-state assumption to efficiently model future ice volumes would be dependent on establishing a reliable assessment of tidewater glacier response time, in order to select an appropriate projection timeframe.

5 Summary remarks

We apply a 1-D (depth-integrated) flowline model to Columbia Glacier that incorporates longitudinal coupling stresses and statistical parameterizations for basal sliding and iceberg calving. A computationally efficient implementation allows Monte Carlo

TCD
6, 893–930, 2012

simulations to be executed over a wide parameter space to produce robust histories and projections of variables of interest, as well as assess the cumulative effect of both parameter and forcing uncertainty. Ensemble selection filters are imposed at: (i) the conclusion of spin-up, to ensure an accurate reproduction of pre-retreat glacier geometry, and (ii) 100 yr into the forcing period, to ensure terminus retreat has initiated. The resultant twice selected ensemble of simulations, with a minimum of parameterizations, reproduces several observed datasets within the uncertainty envelope defined by the ensemble range. These observed datasets include: (i) pre-retreat ice surface elevation profile, (ii) pre-retreat ice surface velocity profile, (iii) contemporary surface mass balance profile and equilibrium line altitude, (iv) time-series of terminus position, and (v) time-series of surface ice velocity at km 50. Iceberg calving rate is well reproduced, except in the vicinity of the K-GN bedrock constriction in the vicinity of km 53 bedrock. A 2-D (plan-view) model is required to resolve the complexities of ice flow in this region. It is not clear, however, how the issue of significant ice density transience, if indeed occurring, may be resolved with a modeling approach predicated on a continuum mechanics momentum balance (i.e. the assumption that ice does not become discontinuous at any time or place).

The ensemble mean projection suggests that Columbia Glacier will achieve a new stable ice geometry c. 2020, by which time iceberg calving rate will have decreased to a dynamic equilibrium value much lower than that observed during the highly transient 1990s and 2000s. Comparison of the pre-retreat (1957) and 2007 glacier geometries with the projected 2100 glacier geometry suggests that, by 2007, Columbia Glacier had already discharged ~ 83 % of the total sea level rise contribution expected by 2100. As the model suggests a short response time (~ 40 yr) between the initial perturbation of the tidewater terminus (c. 1983) and the attainment of a new dynamic equilibrium geometry (c. 2020), this case study highlights the difficulties associated with extrapolating glacier mass loss estimates that are dominated by iceberg calving into the future.

As Columbia Glacier is the single biggest contributor to sea level rise from Alaska, knowledge of its individual response to highly transient contemporary climate change

TCD
6, 893–930, 2012

is essential for predicting the cumulative response of the Alaskan tidewater glacier population. To this end, if the response time of the Alaskan tidewater glacier population can be characterized as similar to that of Columbia Glacier, it may be reasonable to estimate future sea level rise contribution with models assumed to be in steady-state with future climate, rather than fully transient models iteratively solved from the present-day forward. Based on the sheer magnitude of pre-retreat Columbia Glacier, in terms of ice covered area ($\sim 1070\,km^2$), ice thickness (up to 975 m) and bedrock over-deepening (up to 525 m), it has been suggested that Columbia Glacier may be considered analogous to a marine-based ice sheet (Molnia, 2008). Thus, understanding and predicting the response of Columbia Glacier to contemporary climate change likely has value in anticipating the response of the ice sheets.

References

Anderson, J. and Anderson, S.: A Monte-Carlo implementation of the nonlinear filtering problem to produce ensemble assimilations and forecasts, Mon. Weather Rev., 127, 2741–2758, 1999.

Andrews, J. and Miller, G.: Quarternary history of Northern Cumberland Peninsula, Baffin Island, N.W.T., Canada: Part IV: Maps of the present glaciation limits and lowest equilibrium line altitude for North and South Baffin Island, Arctic Alpine Res., 4, 45–59, 1972.

Arendt, A., Echelmeyer, K., Harrison, W., Lingle, C., and Valentine, V.: Rapid wastage of Alaska Glaciers and their contribution to rising sea level, Science, 297, 382–386, doi:10.1126/science.1072497, 2002.

Bamber, J., Riva, R., Vermeersen, B., and LeBrocq, A.: Reassessment of the potential sea-level rise from a collapse of the West Antarctic ice sheet, Science, 324, 901–903, doi:10.1126/science.1169335, 2009.

Bindoff, N., Willebrand, J., Artale, V., Cazenave, A., Gregory, J., Gulev, S., Hanawa, K., Le Quéré, C., Levitus, S., Nojiri, Y., Shum, C., Talley, L., and Unnikrishnan, A.: Observations: oceanic climate change and sea level, in: Climate Change 2007: The Physical Science Basis. Contribution of Working Group I to the Fourth Assessment Report of the Intergovernmental Panel on Climate Change edited by: Solomon, S., Qin, D., Manning, M., Chen, Z.,

TCD
6, 893–930, 2012

Marquis, M., Averyt, K., Tignor, M., and Miller, H., Cambridge University Press, ISBN 978-0521-70596-7, 2007.
Berthier, E., Schiefer, E., Clarke, G., Menounos, B., and Rémy, F.: Contribution of Alaskan glaciers to sea-level rise derived from satellite imagery, Nat. Geosci., 3, 92–95, doi:10.1038/ngeo737, 2010.
Cazenave, A. and Llovel, W.: Contemporary sea level rise, Annu. Rev. Mar. Sci., 2, 145–173, 2010.
Chen, J., Tapley, B., and Wilson, C.: Alaskan mountain glacial melting observed by satellite gravimetry, Earth Planet. Sc. Lett., 248, 368–378, 2006.
Colgan, W., Rajaram, H., Anderson, R. S., Steffen, K., Zwally, H., Phillips, T., and Abdalati, W.: The annual glaciohydrology cycle in the ablation zone of the Greenland Ice Sheet: Part 2. Observed and modeled ice flow, J. Glaciol., 58, 51–64, 2012.
Compo, G. P., Whitaker, J. S., Sardeshmukh, P. D., Matsui, N., Allan, R. J., Yin, X., Gleason, B. E., Vose, R. S., Rutledge, G., Bessemoulin, P., Brönnimann, S., Brunet, M., Crouthamel, R. I., Grant, A. N., Groisman, P. Y., Jones, P. D., Kruk, M., Kruger, A. C., Marshall, G. J., Maugeri, M., Mok, H. Y., Nordli, Ø., Ross, T. F., Trigo, R. M., Wang, X. L., Woodruff, S. D., and Worley, S. J.: The Twentieth Century Reanalysis Project, Q. J. Roy. Meteor. Soc., 137, 1–28, doi:10.1002/qj.776, 2011.
Gagliardini, O. and Zwinger, T.: The ISMIP-HOM benchmark experiments performed using the Finite-Element code Elmer, The Cryosphere, 2, 67–76, doi:10.5194/tc-2-67-2008, 2008.
Gardner, A., Moholdt, G., Wouters, B., Wolken, G., Burgess, D., Sharp, M., Cogley, G., Braun, C., and Labine, C.: Sharply increased mass loss from glacier and ice caps in the Canadian Arctic Archipelago, Nature, 473, 357-360, doi:10.1038/nature10089, 2011.
Jacobs, T., Wahr, J., Pfeffer, W., and Swenson, S.: Recent contributions of glaciers and ice caps to sea level rise, Nature, in press, 2012.
Johannessson, T., Raymond, C., and Waddington, E.: A simple method for determining the response time of glaciers, in: Glacier Fluctuations and Climatic Change, edited by: Oerlemans, J., Kluwer Academic Publishers, ISBN 0-7923-0110-2, 1989.
Kamb, B., Engelhardt, H., Fahnestock, M., and Humphrey, N.: Mechanical and hydrologic basis for the rapid motion of a large tidewater glacier 2. Interpretation, J. Geophys. Res., 99, 15231–15244, 1994.
Kaser, G., Cogley, J., Dyurgerov, M., Meier, M., and Ohmura, A.: Mass balance of glaciers and ice caps: consensus estimates for 1961–2004, Geophys. Res. Lett., 33, L19501,

TCD
6, 893–930, 2012

doi:10.1029/2006GL027511, 2006.
Krimmel, R.: Photogrammetric data set, 1957–2000, and bathymetric measurements for Columbia Glacier, Alaska, US Geol. Surv. Wat. Res. Invest. Rep., 01-4089, 2001.
Lipscomb, W., Bindschadler, R., Bueler, E., Holland, D., Johnson, J., and Price, S.: A community ice sheet model for sea level prediction, EOS T. Am. Geophys. Un., 90, 23, 2009.
Luthcke, S., Arendt, A., Rowlands, D., McCarthy, J., and Larsen, C.: Recent glacier mass changes in the Gulf of Alaska region from GRACE mascon solutions, J. Glaciol., 54, 767–777, 2008.
Machguth, H., Purves, R. S., Oerlemans, J., Hoelzle, M., and Paul, F.: Exploring uncertainty in glacier mass balance modelling with Monte Carlo simulation, The Cryosphere, 2, 191–204, doi:10.5194/tc-2-191-2008, 2008.
Marshall, S., Björnsson, H., Flowers, G., and Clarke, G.: Simulation of Vatnajökull ice cap dynamics, J. Geophys. Res., 110, F03009, doi:10.1029/2004JF000262, 2005.
Mayo, L.: Glacier mass balance and runoff research in the USA, Geograf. Ann., 66, 215–227, 1984.
McNabb, R., Hock, R., O'Neel, S., and Rasmussen, L.: Using surface velocities to infer bed topography: a case study at Columbia Glacier, Alaska, J. Glaciol., submitted, 2012.
Meier, M., Rasmussen, L., Krimmel, R., Oslen, R., and Frank, D.: Photogrammetric determination of surface altitude, terminus position, and ice velocity of Columbia Glacier, Alaska, US Geol. Surv. Prof. Pap., 1258-F, 1985.
Meier, M., Lundstrom, S., Stone, D., Kamb, B., Engelhardt, H., Humphrey, N., Dunlap, W., Fahnestock, M., Krimmel, R., and Walters, R.: Mechanical and hydrologic basis for the rapid motion of a large tidewater glacier 1. Observations, J. Geophys. Res., 99, 15219–15229, 1994.
Meier, M., Dyurgerov, M., Rick, U., O'Neel, S., Pfeffer, W., Anderson, R., Anderson, S., and Glazovsky, A.: Glaciers dominate eustatic sea-level rise in the 21st century, Science., 317, 1064–1067, 2007.
Molnia, B.: Satellite Image Atlas of Glaciers of the World: Alaska, US Geol. Surv. Prof. Pap., 1386-K, 2008.
Nick, F., van der Veen, C., and Oerlemans, J.: Controls on advance of tidewater glaciers: results from numerical modeling applied to Columbia Glacier, J. Geophys. Res., 112, 110–114, doi:10.1029/2006JF000551, 2007.
Nick, F., van der Veen, C., Vieli, A., and Benn, D.: A physically based calving model applied

TCD
6, 893–930, 2012

to marine outlet glaciers and implications for the glacier dynamics, J. Glaciol., 56, 781–794, 2010.
O'Neel, S., Pfeffer, T., Krimmel, R., and Meier, M.: Evolving force balance at Columbia Glacier, Alaska, during its rapid retreat, J. Geophys. Res., 110, F03012, doi:10.1029/2005JF000292, 2005.
Paterson, W.: The Physics of Glaciers, Butterworth-Heinemann, ISBN 0-7506-4742-6, 1994.
Pfeffer, T.: A simple mechanism for irreversible tidewater glacier retreat, J. Geophys. Res., 112, F03S25, doi:10.1029/2006JF000590, 2007.
Price, S., Payne, A., Howat, I., and Smith, B.: Committed sea-level rise for the next century from Greenland ice sheet dynamics during the past decade, P. Natl. Acad. Sci. USA, 108, 8978–8983, 2011.
Radić, V. and Hock, R.: Regional differentiated contribution of mountain glaciers and ice caps to future sea-level rise, Nat. Geosci., 4, 91–94, doi:10.1038/ngeo1052, 2011.
Raper, S. and Braithwaite, R.: Low sea level rise projections from mountain glaciers and ice-caps under global warming, Nature, 439, 311–313, doi:10.1038/nature04448, 2006.
Rasmussen, L., Conway, H., Krimmel, R., and Hock, R.: Surface mass balance, thinning and iceberg production, Columbia Glacier, Alaska, 1948–2007, J. Glaciol., 57, 431–440, 2011.
Rignot, E., Velicogna, I., van den Broeke, M., Monaghan, A., and Lenaerts J.: Acceleration of the contribution of the Greenland and Antarctic ice sheets to sea level rise, Geophys. Res. Lett., 38, L05503, doi:10.1029/2011GL046583, 2011.
Van der Veen, C.: Longitudinal stresses and basal sliding: a comparative study, in: Dynamics of the West Antarctic Ice Sheet, edited by: Van der Veen, C. and Oerlemans, J., D. Reidel Publishing Company, 1987.
Van Leeuwen, P. and Evensen, G.: Data assimilation and inverse methods in terms of a probabilistic formulation, Mon. Weather Rev., 124, 2898–2913, 1996.
Velicogna, I.: Increasing rates of ice mass loss from the Greenland and Antarctic ice sheets revealed by GRACE, Geophys. Res. Lett., 36, L19503, doi:10.1029/2009GL040222, 2009.
Venteris, E.: Evidence for bottom crevasse formation on Columbia Glacier, Alaska, USA, in: Calving Glaciers: Report of a Workshop, edited by: Van der Veen, C., ISSN: 0896-2472, 1997.
Winkelmann, R., Martin, M. A., Haseloff, M., Albrecht, T., Bueler, E., Khroulev, C., and Levermann, A.: The Potsdam Parallel Ice Sheet Model (PISM-PIK) – Part 1: Model description, The Cryosphere, 5, 715–726, doi:10.5194/tc-5-715-2011, 2011.

TCD
6, 893–930, 2012

Table 1. Variable notation.

Variable	Definition (units)
α	basal sliding scaling length (km)
γ	ablation gradient (a^{-1})
ρ	density of ice ($kg\,m^{-3}$)
τ	total driving stress (Pa)
$\overline{\tau}'_{xx}$	depth-averaged longitudinal stress (Pa)
$\mathcal{H}$	calving criterion Heaviside function ( )
A	flow law parameter ($Pa^{-3}\,a^{-1}$)
D	iceberg calving rate ($m^3\,a^{-1}$)
F	channel shape factor ( )
H	ice thickness (m)
H_{2007}	year 2007 ice thickness (m)
H_{2100}	year 2100 ice thickness (m)
Q	ice discharge ($m^3\,a^{-1}$)
Q_{term}	terminus ice discharge ($m^3\,a^{-1}$)
T	air temperature (K)
V	ice volume (m^3)
b	annual surface mass balance ($m\,a^{-1}$)
b_{max}	maximum annual surface mass balance ($m\,a^{-1}$)
g	gravitational acceleration ($m\,s^{-2}$)
k	dimensional coefficient ($m\,a^{-1}$)
n	flow law exponent ( )
t	time (a)
u_{b}	basal sliding velocity ($m\,a^{-1}$)
u_{s}	ice surface velocity ($m\,a^{-1}$)
w	flowband width (m)
x	flowline position downstream (m)
x_{80}	80 m surface elevation flowline position (m)
x_{term}	terminus flowline position (m)
z	elevation (m)
z_{ela}	equilibrium line altitude (m)
z_{s}	ice surface elevation (m)

TCD
6, 893–930, 2012

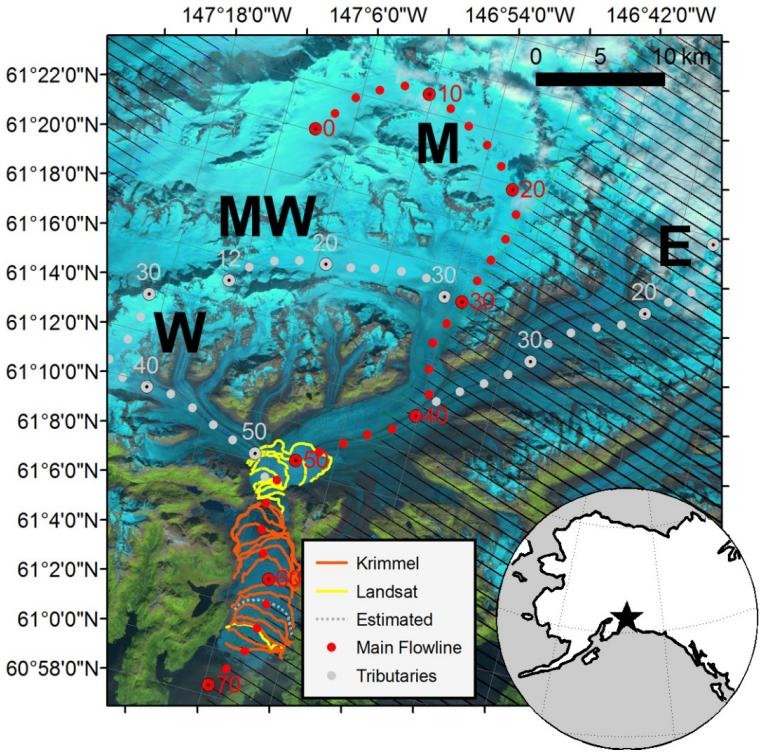

Fig. 1. A Landsat 7 image of Columbia Glacier acquired 23 August 2010 with the curvilinear coordinate system (ζ in km) employed by Meier et al. (1985) to describe the "main" flowline (M) and its tributaries, "west" (W), "main-west" (MW) and "east" (E), overlaid. An updated record of annual terminus position over the 1984 to 2010 period is also shown (Krimmel, 2001). Inset: Location of Columbia Glacier in Alaska.

TCD
6, 893–930, 2012

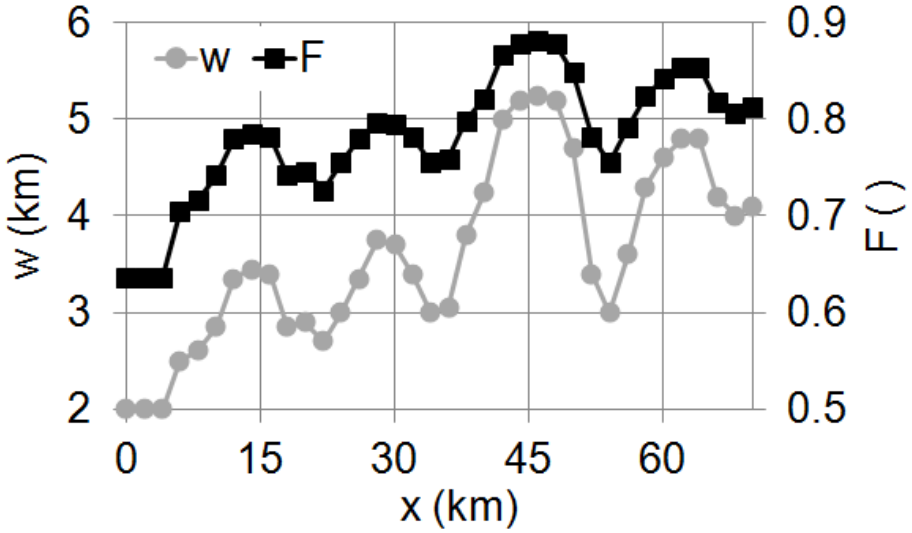

Fig. 2. Observed glacier width (w) profile at Columbia Glacier (Meier et al., 1985) and the corresponding spatially variable shape factor (F; Paterson, 1994, p. 269) applied to the ice flow model in this study.

TCD
6, 893–930, 2012

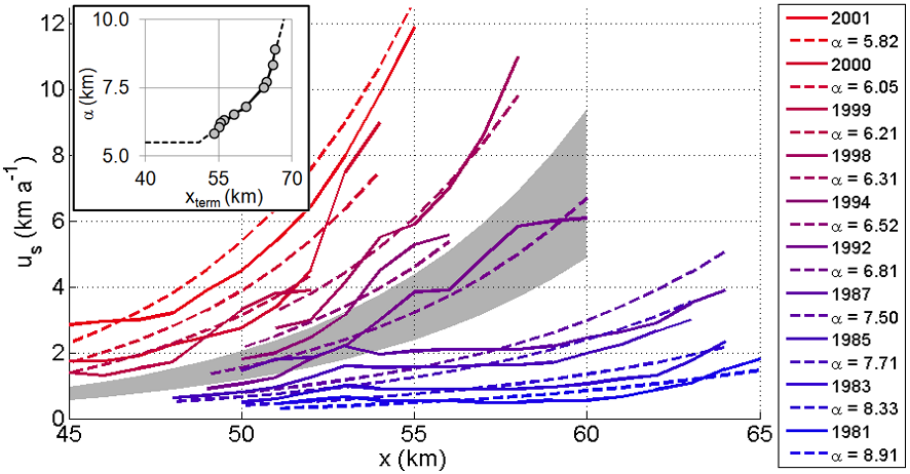

Fig. 3. Observed ice surface velocity (u_s) profiles at Columbia Glacier over the 1981 to 2001 period (solid lines; Pfeffer, 2007) and their corresponding parameterizations (dashed lines; Eq. 5) using differing values of exponential length scale (α). Grey shading denotes $\alpha \pm 0.25$ km around the 1992 profile. Inset: The empirical relation between exponential sliding length scale (α) and terminus position (x_{term}) used in this study.

TCD
6, 893–930, 2012

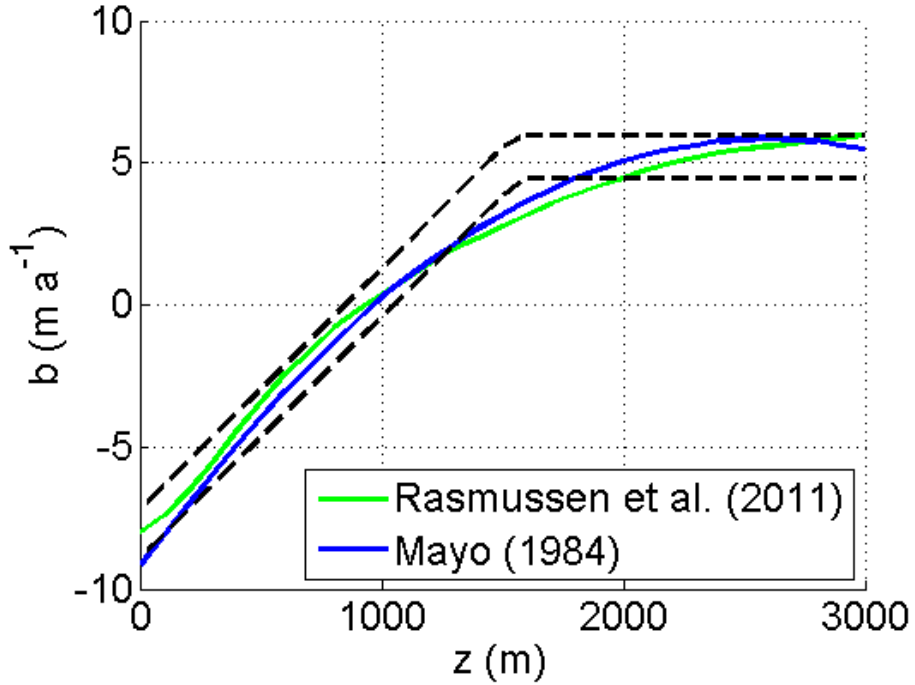

Fig. 4. Observed relation between surface mass balance (b) and elevation (z) at Columbia Glacier (solid lines; Mayo, 1984; Rasmussen et al., 2011), and the parameterized range (dashed lines; Eq. 6) used in this study.

TCD
6, 893–930, 2012

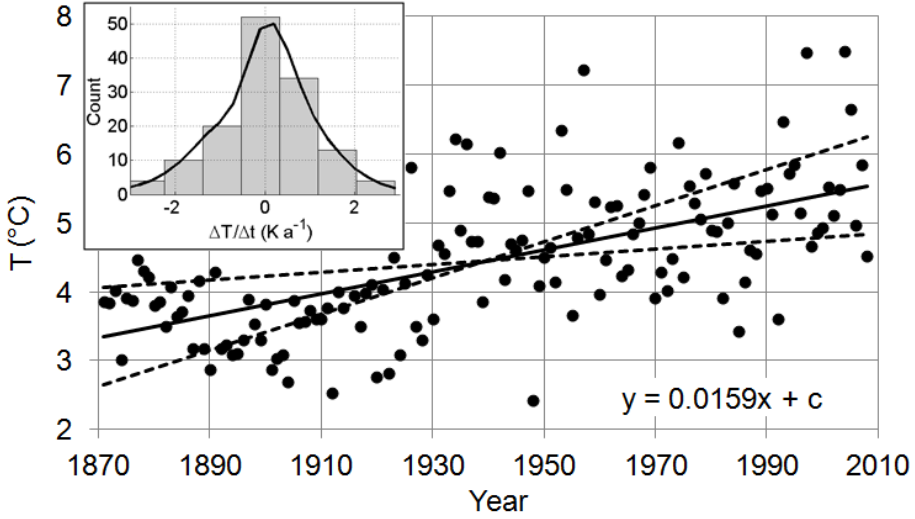

Fig. 5. Mean melt season (1 April to 30 September) 900 mb air temperature (T) over the 1871 to 2008 period at Columbia Glacier extracted from the 20th Century Reanalysis V2 data provided by NOAA/OAR/ESRL PSD (Compo et al., 2011). Inset: Corresponding histogram and non-parametric distribution of annual variability in 900 mb air temperature ($\Delta T/\Delta t$).

TCD
6, 893–930, 2012

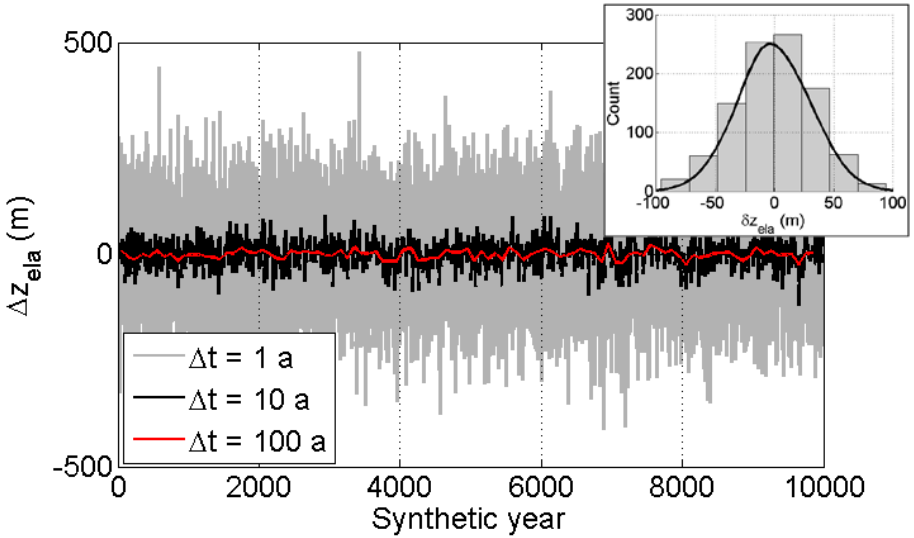

Fig. 6. Synthetic annual ($\Delta t = 1$ a) variability in equilibrium line altitude (Δz_{ela}) over 10 000 yr, generated using the $\Delta T/\Delta t$ distribution shown in Fig. 5 and a lapse rate ($\Delta T/\Delta z$) of 6.7 K km^{-1}. The corresponding decadal and centurial variability are also shown ($\Delta t = 10$ and 100 a, respectively). Inset: Histogram and normal distribution (mean = 0 m; standard deviation = 30 m) of decadal z_{ela} perturbations (δz_{ela}).

TCD
6, 893–930, 2012

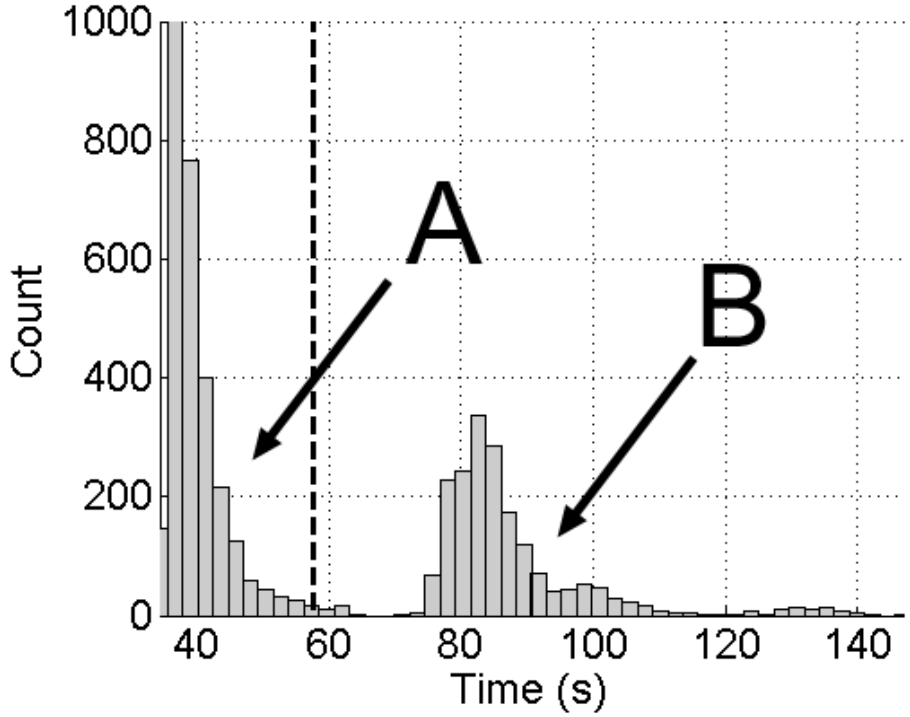

Fig. 7. Histogram of processor time per simulation of the 5000 Monte Carlo simulations. The dashed line denotes the ensemble mean (58 s). The bimodal distribution is due to the greater computational requirements of simulations selected to carry forward into transient forcing following spin-up (B) in comparison to those that were not selected (i.e. discarded following spin-up; A).

TCD
6, 893–930, 2012

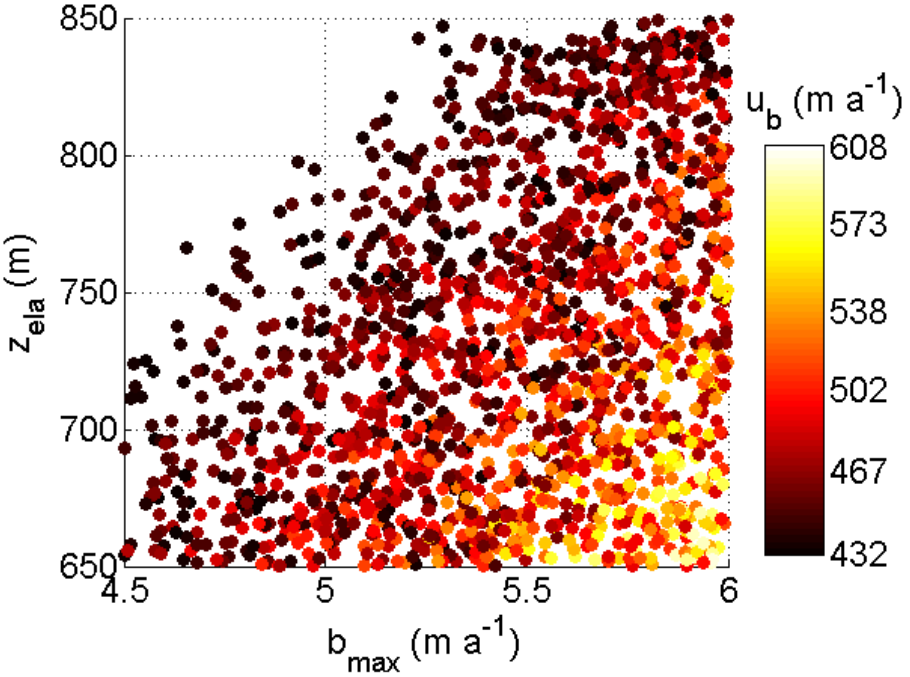

Fig. 8. Equilibrium line altitude (z_{ela}), maximum surface mass balance (b_{max}; or accumulation) and basal sliding velocity (mean between km 50 and 60; u_b) in the selected ensemble of 1707 simulations.

TCD
6, 893–930, 2012

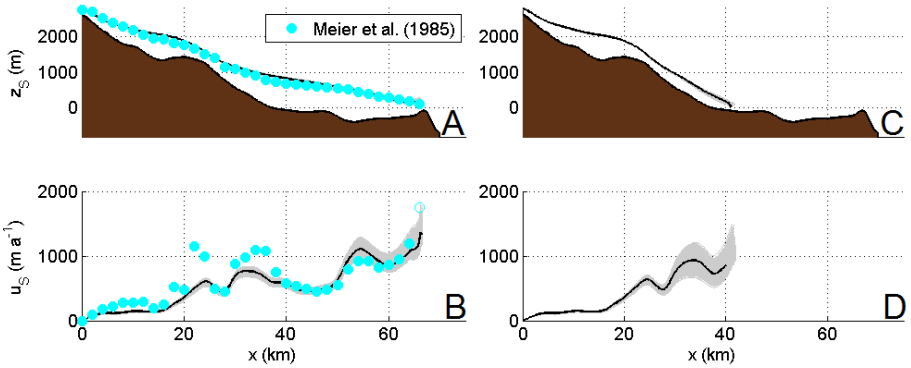

Fig. 9. Modeled (grey lines with ensemble mean in black) and observed (points; Meier et al., 1985) ice surface elevation (z_s) and ice surface velocity (u_s) along the Columbia Glacier main flowline (x) in 1977/78 (pre-retreat; **A** and **B**) and in 2100 (post-retreat; **C** and **D**).

TCD
6, 893–930, 2012

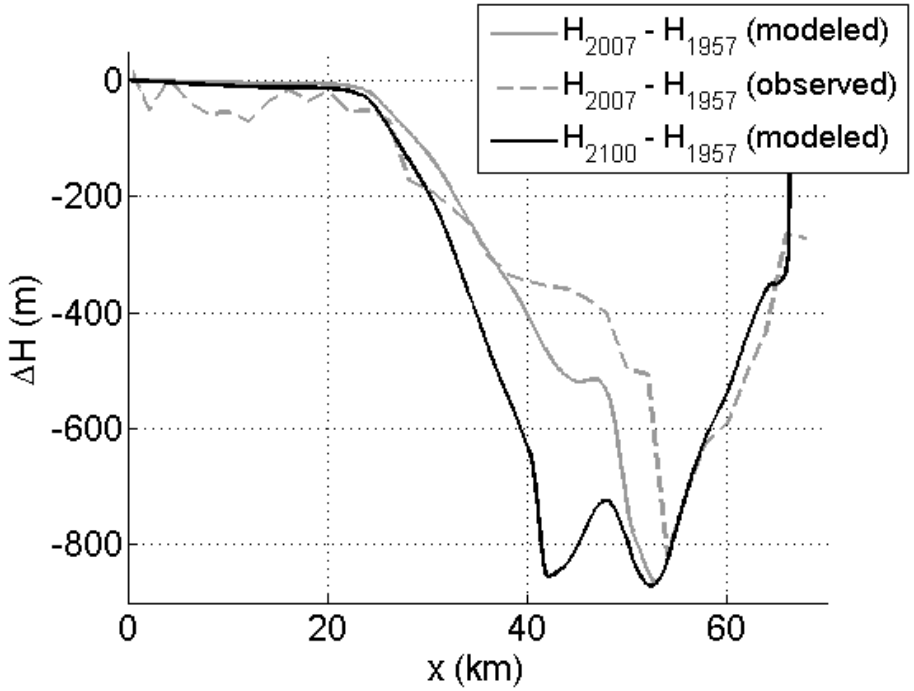

Fig. 10. Observed (McNabb et al., 2012) and modeled ensemble mean change in ice thickness (ΔH) along the Columbia Glacier main flowline (x) between 1957 and 2007, and modeled ensemble mean change in ice thickness between 1957 and 2100.

TCD
6, 893–930, 2012

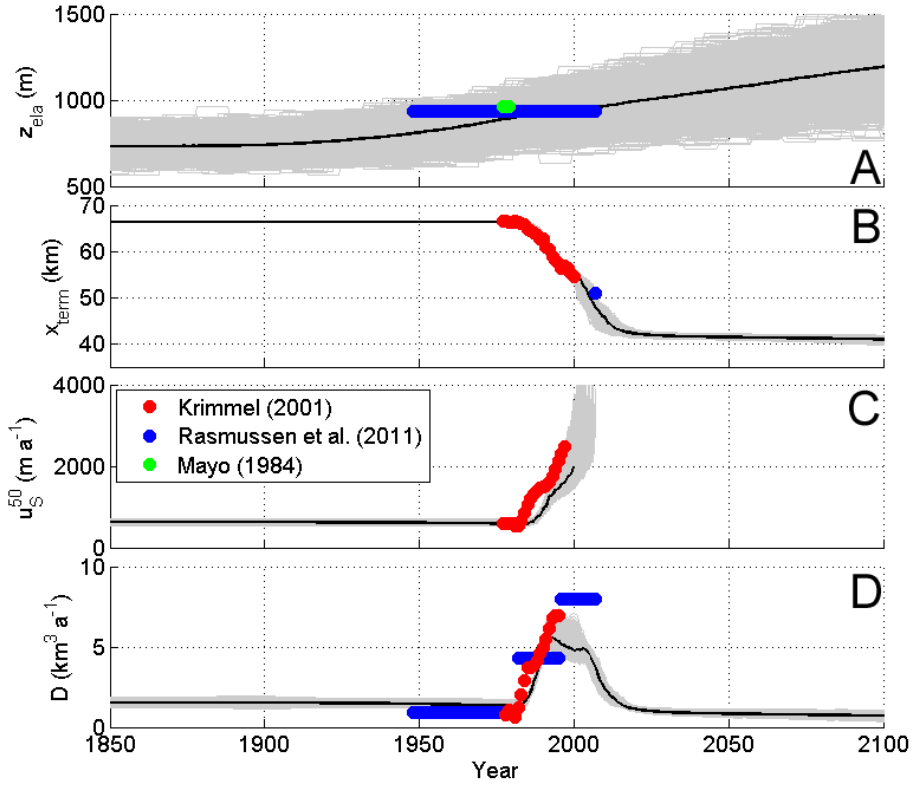

Fig. 11. Modeled (grey lines with ensemble mean in black) and observed (points; Mayo, 1984; Krimmel, 2001; Rasmussen et al., 2011) time-series of equilibrium line altitude (z_{ela}; **A**), terminus position (x_{term}; **B**), ice surface velocity at km 50 (u_s^{50}; **C**) and calving flux (D; **D**) at Columbia Glacier over the 1850 to 2100 period.

TCD
6, 893–930, 2012

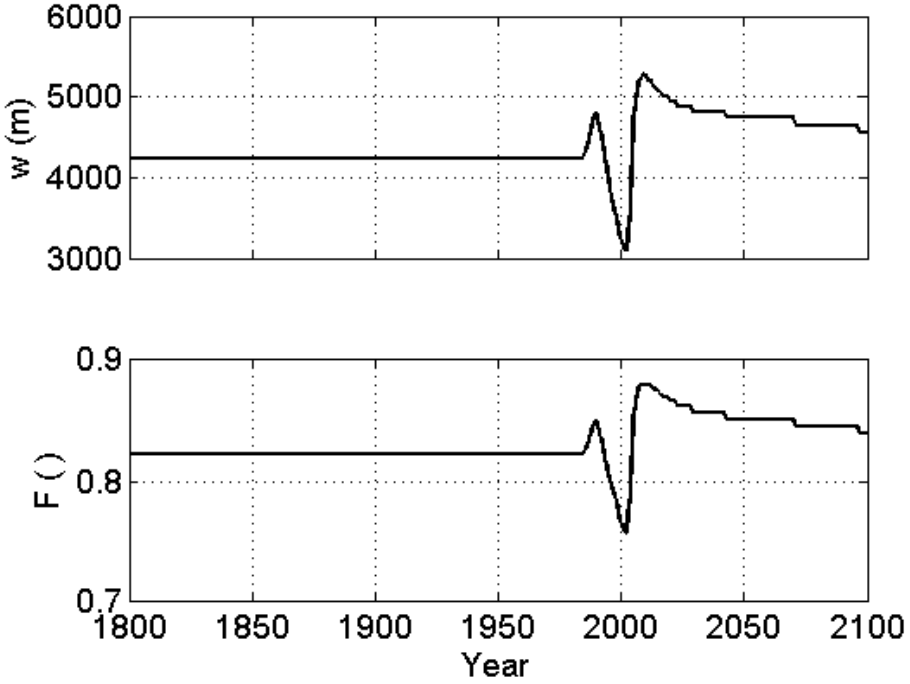

Fig. 12. Ensemble mean time-series of glacier width (w) and shape factor (F) at the terminus.

TCD
6, 893–930, 2012